Available online at www.sciencedirect.com
SCIENCE DIRECT
Bioorganic & Medicinal Chemistry Letters 16 (2006) 573–580
Bioorganic & Medicinal Chemistry Letters

Isolation and cholinesterase-inhibition studies of sterols from *Haloxylon recurvum*

Ejaz Ahmed, Sarfraz A. Nawaz, Abdul Malik* and M. Iqbal Choudhary

International Center for Chemical Sciences, HEJ Research Institute of Chemistry, University of Karachi, Karachi-75270, Pakistan

Received 23 July 2005; revised 4 October 2005; accepted 17 October 2005
Available online 7 November 2005

Abstract—Haloxysterols A–D (**1**–**4**), new C-24 alkylated sterols, have been isolated from the chloroform soluble fraction of *Haloxylon recurvum*, along with five known sterols **5**–**9**, which are reported for the first time from this species. Their structures were determined by means of 1D- and 2D-NMR techniques. Compounds **1**–**9** inhibited cholinesterase enzymes in a concentration-dependent manner with K_i values ranging between 0.85–25.5 and 1.0–19.0 μM against acetylcholinesterase (AChE; EC 3.1.1.7) and butyrylcholinesterase (BChE; EC 3.1.1.8) enzymes, respectively. Lineweaver–Burk, Dixon plots and their secondary replots indicated that compounds **1**–**9** are non-competitive inhibitors of both AChE and BChE enzymes.

Haloxylon recurvum Bunge ex Boiss belongs to the family Chenopodiaceae which comprises of 100 genera and 1200 species.[1] In Pakistan, this family is represented by 35 genera. Only five species of *Haloxylon* are found in Pakistan.[2] *H. recurvum* is a perennial shrub with glabrous leaves. It is widely distributed in Turkey, Syria, Iraq, Iran, Afghanistan, Kashmir, India, and Central Asia.[3] The plant is traditionally reported to be applied externally on insect stings. The ash of the plant is used for internal ulcers, while a decoction of the whole is used for the treatment of a variety of neural disorders.[4,5] No phytochemical work has so far been reported on this species. The methanolic extract of *H. recurvum*[6] showed strong toxicity in brine shrimp lethality test. On further pharmacological screening it showed strong inhibition against cholinesterase enzyme. This prompted us to carry out bioassay directed isolation studies on this plant. We now report the isolation[7] and structure elucidation of four new sterols named as haloxysterols A–D (**1**–**4**),[8–11] along with sterols **5**–**9**,[12–16] reported for the first time from this species.

The discovery of cholinesterase inhibitors has been a challenging area of pharmaceutical research due to the involvement of cholinesterase enzymes in Alzheimer's disease and other related dementias. AChE is a key component of cholinergic brain synapses and neuromuscular junctions. The major biological role of the enzyme is the termination of impulse transmission by rapid hydrolysis of the cationic neurotransmitter acetylcholine.[17] According to the cholinergic hypothesis, the memory impairment in the patients with senile dementia of *Alzheimer's* type results from a deficiency in cholinergic function in the brain.[18] Hence, the most promising therapeutic strategy for activating central cholinergic functions has been the use of cholinomimetic agents. The aim of AChE inhibitors is to boost the endogenous levels of acetylcholine in the brains of Alzheimer's disease patients and thereby, to increase cholinergic neurotransmission. The role of BChE in normal aging and brain diseases is still elusive. BChE has been found in significantly higher quantities in Alzheimer's plaques than in normal age-related non-demented brains.[19]

We have previously reported a number of new natural inhibitors of cholinesterase enzymes, isolated from medicinally important plants.[20,21] Continuing our efforts to discover new inhibitors of therapeutically significant enzymes through high-throughput screening assays, we found sterols **1**–**9** with efficacious cholinesterase inhibitory potential.

The MeOH extract of *Haloxylon recurvum* was divided into *n*-hexane, chloroform, ethyl acetate, *n*-butanol, and water soluble fractions. The chloroform soluble fraction, which showed major inhibitory activity against

Keywords: *Haloxylon recurvum*; Chenopodiaceae; Sterols; Enzyme inhibition; Acetylcholinesterase; Butyrylcholinesterase.
* Corresponding author. Tel.: +92 21 4824926; fax: +92 21 4819018/4819019, UAN # 111 222 292x139; e-mail: abdul.malik@iccs.edu

0960-894X/$ - see front matter © 2005 Elsevier Ltd. All rights reserved.
doi:10.1016/j.bmcl.2005.10.042

cholinesterase enzymes, was further subjected to chromatographic techniques to afford four new sterols named as haloxysterols A–D (**1**–**4**), along with five known sterols, namely 5α,8α-epidioxy-(24*S*)-ethyl-cholesta-6,9(11),22(*E*)-triene-3β-ol (**5**),[12] (24*S*)-ethyl-cholesta-7,9(11),22(*E*)-triene-3β-ol (**6**),[13] lawsaritol (**7**),[14] 24-ethyl-cholest-7-ene-3,5,6-triol (**8**),[15] and 24-ethyl-cholest-6-ene-3,5-diol (**9**),[16] respectively, reported for the first time from this species.

Haloxysterols A–D (**1**–**4**) gave positive Salkowski and Lieberman. Burchard tests for sterols. Their IR spectra showed the presence of hydroxyl and olefinic functionalities, except for haloxysterol D (**4**) which did not show unsaturation. A hydroxyl group could be assigned to the usual C-3 position on biogenetic analogy, ^{1}H–^{1}H COSY, HMBC correlations and comparison of NMR spectral data with those of known sterols. Its stereochemistry was assigned β and equatorial based on larger coupling constant of oxymethine proton at C-3. An ethyl group was invariably observed at C-24 [δ 0.84–0.87 (3H, d, J = 6.78–7.2 Hz, H-29) and δ 1.24–1.29 (2H, m H-28)]. The '*R*' configuration could be assigned to it in haloxysterols A–D based on comparison of ^{13}C NMR chemical shift of the side chain with stigmasterol and schleicherastatin **1** (see Fig. 1).[22–25]

Haloxysterol A (**1**) was obtained as colorless crystals, mp 171–172 °C, $[\alpha]_D^{20}$ −63.5 (*c* 1.0, $CHCl_3$). The HREIMS showed molecular ion peak at *m*/*z* 446.3785 consistent with the molecular formula $C_{29}H_{50}O_3$. The intense peak at *m*/*z* 289.2151 ($C_{19}H_{29}O_2$) was due to the loss of $C_{10}H_{19}O$ side chain indicating the presence of two hydroxyl and one olefinic bonds in the steroidal nucleus and an oxygen atom in the side chain. The diagnostic fragment at *m*/*z* 57.0325 (C_3H_5O) was characteristic of Δ^5-3-ol type of sterols.[22] The ^{1}H NMR spectrum showed the proton of the trisubstituted double bond at δ 5.34 (br d, J = 5.1 Hz). The oxymethine protons were observed at δ 3.99, 3.84, and 3.45, respectively. The most

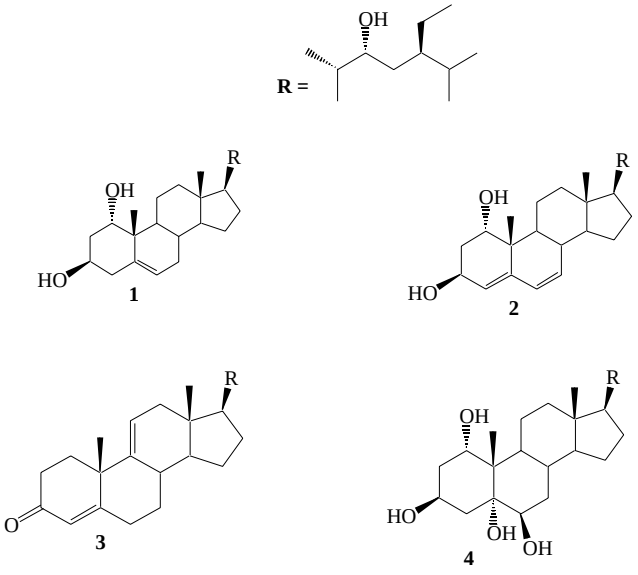

Figure 1. Structures of haloxysterols A (**1**), B (**2**), C (**3**), and D (**4**).

downfield oxymethine proton at δ 3.99 showed connectivity to four neighboring protons in the ^{1}H–^{1}H COSY spectrum and hence could be assigned to C-3. Two of these protons at δ 1.87 and 1.76 further showed connectivity to another oxymethine proton at δ 3.84 thereby allowing us to assign both these protons to C-2 and the hydroxyl group to C-1. The α and axial configuration was assigned to the latter on the basis of smaller coupling constant (J = 2.6 and 4.9 Hz) of H-1β. The relative positions of double bond and hydroxyl groups were further confirmed by selective decoupling experiments and HMBC correlations (Fig. 2). The position of the remaining hydroxyl group in the side chain could be confirmed at C-22 by a comparison of chemical shifts of the side chain with those of related sterols.[22,23] In ^{1}H–^{1}H correlated spectroscopy, the oxymethine proton at δ 3.45 showed connectivity with three other protons including H-20 at δ 1.7. The HMBC correlations (Fig. 2) of the side chain also confirmed the position of the hydroxyl group at C-22. Its α-configuration could be assigned on the basis of NOEs between protons of C-17, C-20, and C-22. The ^{13}C NMR spectrum and HMBC correlations were in exact agreement with the assigned structure of haloxysterol A (**1**) as (24*R*)-ethyl-cholest-5-ene-1α,3β,22α(22*R*)-triol.

Haloxysterol B (**2**) was obtained as colorless crystals mp 158–159 °C, $[\alpha]_D^{20}$ −55 (*c* 0.75, $CHCl_3$). The HREIMS showed molecular ion peak at *m*/*z* 444.3638 consistent with the molecular formula $C_{29}H_{48}O_3$. The IR, mass, and ^{1}H NMR spectra were very similar to those of haloxysterol A, except for the presence of an additional disubstituted double bond in the steroidal nucleus. Both the proton and ^{13}C NMR chemical shifts of rings C and D were similar to **1**, hence both the double bonds must be present in rings A and B. Since the conjugation of these double bonds was evident from the UV spectrum showing λ_{max} at 232, 240, and 248 nm, the possible loci were at C-4 and C-6. These relative positions could be confirmed through ^{1}H–^{1}H COSY correlations; H-3 showing connectivity to C-4 olefinic protons at δ 5.75, C-7 olefinic proton at δ 5.57 showing connectivity to both C-6 olefinic proton at δ 5.80 and H-8 at δ 2.09. The ^{13}C NMR spectrum and HMBC correlations (Fig. 2) were in agreement with the assigned structure of haloxysterol B (**2**) as (24*R*)-ethyl-cholesta-4,6-diene-1α,3β,22α(22*R*)-triol.

Haloxysterol C (**3**) crystallized from methanol, mp 195 °C, $[\alpha]_D^{25}$ −75 (*c* 0.26, MeOH). Its HREIMS showed molecular ion peak at *m*/*z* 426.3471 consistent with the molecular formula $C_{29}H_{46}O_2$, showing the presence of seven degrees of unsaturation. The UV spectrum showed absorption maximum at 238 nm which is characteristic for Δ^4-3-oxo-steroidal skeleton,[26] while IR spectrum showed absorption bands at 3390, 1686, and 1610 cm^{-1} indicating the presence of hydroxyl, α,β-unsaturated cyclic ketone, and the double bond, respectively. The ^{1}H NMR spectrum showed the presence of characteristic singlet for the olefinic proton at δ 5.17 indicative of Δ^4-unsaturation.[27] Broad-band ^{13}C NMR spectrum including DEPT experiments indicated 29 signals including six methyl, nine methylene, nine methine,

and five quaternary carbons. The downfield signal at δ 199.6 was due to Δ^4-3 one system. Two downfield signals at δ 123.7 and 171.6 were assigned to C-4 and C-5, respectively. Further comparison of the data with those of haloxysterol A (**1**) revealed similarity of the side chain. The position of the other double bond in the steroidal nucleus was assigned 9(11) based on the mass fragments at *m*/*z* 174 and 188,[28] and the characteristic chemical shift of C-18 protons.[29] In HMBC experiments (Fig. 2), the proton at position 4 of the steroidal nucleus showed ^2J correlations with C-2, C-10, and C-6, while the H-11 showed the same HMBC correlations as observed earlier in the case of haloxysterol A. On the basis of these evidences, compound (**3**) was assigned the structure 22 α-hydroxy-(24*R*)-ethyl-cholesta-4,9(11)dien-3 one.

Haloxysterol D (**4**) crystallized from methanol as colorless crystals, mp 250–251 °C, $[\alpha]_D^{25}$ −35.5 (*c* 0.73, MeOH). It showed pseudomolecular ion peaks at *m*/*z* 481 $[M+H]^+$ and 479 $[M-H]^-$ in the positive and negative mode FABMS, respectively. The HREIMS showed $[M-H_2O]^+$ peak at *m*/*z* 462.3735 corresponding to the composition $C_{29}H_{50}O_4$. The mass spectrum further showed fragments at *m*/*z* 323.2222 ($C_{19}H_{31}O_4$) [M−side chain]$^+$, 322.2143 ($C_{19}H_{30}O_4$) [M−side chain−H]$^+$, and 305.2037 ($C_{19}H_{28}O_3$) $[M-\text{side chain}-H_2O]^+$. The peaks at *m*/*z* 282.1825 ($C_{16}H_{26}O_4$), 264.1705 ($C_{16}H_{24}O_3$), 246.0915 ($C_{16}H_{22}O_2$), and 228.1522 ($C_{16}H_{20}O$) were derived by a typical ring-D Fission with proton migration and stepwise H_2O losses.[15] It was, therefore, evident that the four oxygen functions in the molecule were located on the rings A, B, and C, while the remaining oxygen function was present in the side chain.

Decoupling experiments clarified the relation among the C-1 to C-4 protons and confirmed an α-OH located at C-1. Irradiation of the symmetrical multiplets at δ 4.14–4.29, attributable to H-3, simplified simultaneously the H_2-2 signals at 1.78–1.82 and the H_2-4 signals at 2.04–2.14. Both the C-2 and C-4 methylene signals showed large coupling constants 14 and 12.5 Hz, respectively, with H-3α, which indicated a vicinal diaxial coupling. Thus, the H-3 was assigned the α and axial configuration. Irradiation of the triplet at δ 3.81 (1H, J = 4.0 Hz) caused simplification of the H_2-2 signals showing the presence of another hydroxyl at C-1 in α and axial orientation.

In general, the C-3 protons of 3-hydroxy-A/B *trans*-steroids resonate at 3.58 (axial) and 4.15 ppm (equatorial).[30] Its downfield multiplet at 4.08 ppm is characteristic of 3β-hydroxysterols bearing a 5α-hydroxyl group.[31] The most downfield signal at δ 4.29 revealed that the H-3α must be subjected to a double 1, 3 diaxial interaction with two axial hydroxyl groups at C-1 and C-5, establishing the 1α-OH and 5α-OH configuration.

In the ^{1}H NMR spectrum of (**4**) in pyridine-d_5, the 18 and 19 angular methyl resonances occurred at δ 0.75 and 1.57 ppm, respectively. On comparison of the spectra that had been determined in $CDCl_3$ and pyridine-d_5, a large pyridine-induced deshielding was observed for Me-19, thus indicating the presence of a hydroxyl group near Me-19 but remote from Me-18. The 6β position is the only position to accord with this demand, and thus the third secondary hydroxyl group must be located at the 6β position. In addition, the small values of coupling constants (J = 1 and 3.5 Hz) indicated the presence of an

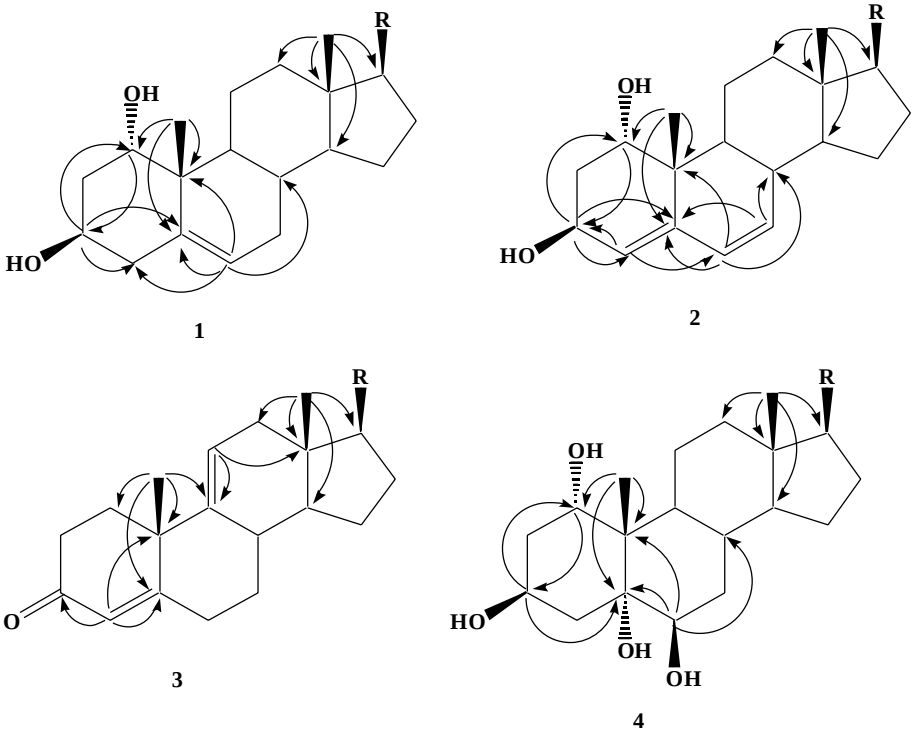

Figure 2. Important HMBC correlations of haloxysterols A–D (**1**–**4**).

equatorial hydrogen at C-6 (α orientation). The configuration of C-20 and C-22 (*S* and *R*, respectively) was suggested by the NOEs from H-21 to H-12α, H-17, H-18, and OH-22; from H-20 to H-18; and from H-22 to H-16α and H-20. The utility of the ^{13}C NMR chemical-shift difference of C-20 has been reported to differentiate (22*R*)- and (22*S*)-hydroxysterols, when the observed chemical shifts of C-20 were δ 42.6 and 40.3, respectively.[25] Application of this chemical shift rule for **4** (the chemical shift at δ 42.9 for C-20) supported the '*R*' configuration of C-22 described above (Tables 1 and 2). Thus, haloxysterol D (**4**) was assigned the structure 24*R*-ethyl-cholesta-1α,3β,5α,6β,22α-pentanol.

Compounds **1**–**9** were studied for their cholinesterase inhibitory potential[32–39] and all of them were found to inhibit AChE and BChE enzymes in a concentration-dependent manner with K_i values ranging from 0.85 to 25.5 μM and 1.0 to 19.0 μM against AChE and BChE, respectively. The K_i values were calculated in three ways; first, the slopes of each line in the Lineweaver–Burk plot were plotted against different concentrations of compounds, second the $1/V_{maxapp}$ was calculated by plotting different fixed concentrations of substrates (ATCh or BTCh) versus ΔV in the presence of different fixed concentrations of compounds in the respective assays of AChE or BChE. Then K_i was calculated by plotting different concentrations of inhibitor versus $1/V_{maxapp}$. K_i is the intercept on the *x*-axis. In the third method, K_i was directly measured from the Dixon plot as an intercept on the *x*-axis. Determination of the inhibition type is important to understand the mechanism of enzyme action and the inhibitor binding sites. Lineweaver–Burk, Dixon plots, and their replots indicated the non-competitive type of inhibition of compounds **1**–**9** against AChE and BChE enzymes, as there was a decrease in V_{max} without affecting the affinity (K_m values) of the AChE or BChE towards the substrates (ATCh or BTCh), respectively. In other words, these inhibitors and substrate (ATCh or BTCh) bind randomly and independently at the different sites of AChE or BChE, respectively. The similar binding mode of compounds **1**–**9** is not surprising because all of them have almost similar structures with minor differences only in the basic skeleton of the compounds. It also indicated that the observed inhibition depends only on the concentration of inhibitors and dissociation constant (K_i). The IC_{50}, K_i, values and the type of inhibition are listed in Table 3. The graphical presentation of steady-state inhibition data of compound **5** for AChE and BChE has been presented in Figure 3.

The inhibitory potential ($K_i = 7.6 \pm 0.01$ μM) of compound **1** can be the cumulative effect of hydrogen bonding and π–π stacking interactions. The hydroxyl moieties present can be involved in hydrogen bonding with the amino acid residues of the active site of the AChE. Similarly, double bond present in ring B can

Table 1. ^1H NMR Data of compounds **1**–**3** ($CDCl_3$) and **4** (Py-d_5)

Position	1	2	3	4
1	3.84 (dd, 2.6, 4.9)	3.88 (dd, 2.4, 4.8)	2.04 (m) 1.71 (m)	3.99 (dd, 1.8, 4.2)
2	2.21 (m), 1.85 (m)	2.21 (m), 1.85 (m)	2.55 (m) 2.15 (m)	2.21 (m) 1.85 (m)
3	3.99 (m)	4.21 (m)	—	4.85 (m)
4	2.38 (dd, 12.5, 5.1) 2.25 (dd, 12.5, 11.6)	5.75 (d, 4.1)	5.17 (s)	2.38 (dd, 12.5, 5.1) 2.25 (dd, 12.5, 11.6)
5	—	—	—	—
6	5.34 (br d, 5.1)	5.80 (br d, 10.2)	1.55 (m) 1.20 (m)	4.15 (dd, 1, 3.5)
7	1.65 (m)	5.57 (dd, 10.2, 2.6)	1.66 (m) 1.20 (m)	1.65 (m)
8	1.78 (m)	1.79 (m)	1.79 (m)	1.78 (m)
9	1.35 (m)	1.34 (m)	1.34 (m)	1.35 (m)
10	—	—	—	—
11	1.71 (m), 2.78 (m)	1.66 (m), 2.70 (m)	5.53 (br d, 6.4)	1.71 (m), 2.78 (m)
12	1.02 (m), 2.01 (m)	1.04 (m), 2.01 (m)	1.04 (m) 2.01 (m)	1.02 (m), 2.01 (m)
13	—	—	—	—
14	1.13 (m)	1.11 (m)	1.11 (m)	1.13 (m)
15	1.55 (m)	1.59 (m)	1.59 (m)	1.55 (m)
16	1.38 (m) 1.27 (m)	1.35 (m) 1.25 (m)	1.35 (m) 1.25 (m)	1.38 (m) 1.27 (m)
17	1.19 (m)	1.18 (m)	1.18 (m)	1.19 (m)
18	0.71 (s)	0.75 (s)	0.68 (s)	0.75 (s)
19	1.11 (s)	1.11 (s)	0.86 (s)	1.57 (s)
20	1.73 (m)	1.73 (m)	1.73 (m)	1.73 (m)
21	0.94 (d, 6.8)	1.00 (d, 6.0)	1.08 (d, 6.2)	1.0 (d, 6.0)
22	3.45 (ddd, 10.8, 3.4,1.7)	3.76 (ddd, 10.6, 3.2, 1.5)	3.76 (m)	3.73 (m)
23	1.04 (dd, 13.5,10.5), 1.27 (m)	1.04 (dd, 13.5, 10.5) 1.27 (m)	1.04 (m) 1.27 (m)	1.04 (dd, 13.5,10.5), 1.27 (m)
24	1.38 (m)	1.38 (m)	1.38 (m)	1.35 (m)
25	1.78 (m)	1.78 (m)	1.78 (m)	1.75 (m)
26	0.90 (d, 6.8)	1.04 (d, 6.8)	0.99 (d, 6.8)	1.04 (d, 6.5)
27	0.90 (d, 6.8)	1.04 (d, 6.8)	0.99 (d, 6.8)	1.04 (d, 6.5)
28	1.27 (m), 1.39 (m)	1.27 (m), 1.39 (m)	1.27 (m) 1.39 (m)	1.26 (m), 1.38 (m)
29	0.88 (t, 7.2)	0.84 (t, 7.0)	0.88 (t, 7.0)	0.99 (t, 6.9)

The coupling constants are given in Hz.

Table 2. ^{1}H NMR data of compounds **1**–**3** ($CDCl_3$) and **4** (Py-d_5)

Position	1	2	3	4
1	75.9	74.0	35.7	75.9
2	39.1	38.9	38.9	39.1
3	65.6	67.9	199.6	66.8
4	42.5	118.1	123.7	42.5
5	140.0	140.0	171.6	79.1
6	124.1	132.8	32.9	76.8
7	39.5	136.2	32.1	39.5
8	32.0	36.4	36.0	32.0
9	50.4	42.5	146.2	50.4
10	37.1	40.9	39.5	37.1
11	21.5	21.4	118.5	21.5
12	40.8	41.1	42.1	40.8
13	43.0	41.8	42.8	43.0
14	56.9	55.5	54.6	56.9
15	25.8	25.2	24.8	25.8
16	29.5	29.9	28.8	29.5
17	56.6	57.6	56.9	56.6
18	12.2	12.8	12.9	12.2
19	19.4	17.9	19.3	19.4
20	42.4	43.0	39.9	42.4
21	12.8	12.6	12.6	12.8
22	72.0	72.1	73.0	72.1
23	29.7	29.8	29.5	29.7
24	41.6	41.9	42.0	41.6
25	28.9	28.9	28.6	28.9
26	17.8	18.0	18.0	17.8
27	20.5	19.9	19.5	20.5
28	23.5	23.4	22.9	23.5
29	11.9	11.9	12.2	11.9

have π–π stacking interactions with amino acid residues in the active center of AChE. The hydrogen bonding and π–π stacking interactions seem to be the main stabilizing factors of AChE–**1** compound complex, increasing the affinity of the compound **1** toward the AChE. The compound **2** displayed ($K_i = 0.85 \pm 0.001$ μM) highest inhibitory potential the rationale may stem from the fact that the compound **2** has one extra double bond in the ring A, the double bonds can be involved in the π–π stacking interactions, and that these interactions are energetically very favorable to make the AChE–**2** complex stable and consequently the high potency of the compound **2**. The oxygen of carbonyl moiety of compound **3** ($K_i = 1.1 \pm 0.05$ μM) can make a strong hydrogen bond with the amino acid residues in the active site, additional π–π stacking interactions of compound **3** with the active site amino acid residues of AChE, and operational π–π stacking interactions can further strengthen the AChE–**3** complex. Compound **5** displayed least inhibitory potential ($K_i = 25.5 \pm 0.01$ μM) among the series of sterols reported in this article which may be due to the oxygen bridging that can shield the π–π stacking interaction of the amino acid residues in the active center of AChE, the only driving force in the **5**–AChE complex seems to be the hydrogen bonding. Potency decreased (Compound **6**, $K_i = 20.6 \pm 0.02$ μM) with the decrease of –OH groups and olefinic double bonds. There is, slight increase in the activity with the availability of hydroxyl group and olefinic double bond (Compound **7**, $K_i = 16.1 \pm 0.01$ μM). Increase in the number of hydroxyl groups further increased the activity (Compound **8**, $K_i = 12.6 \pm 0.04$ μM). A sharp increase in the inhibitory potential occurred when both hydrogen bonding and π–π stacking interaction were operative (Compound **9**, $K_i = 4.0 \pm 0.09$ μM).

In case of BChE inhibition, the potential of compound **1** ($K_i = 4.5 \pm 0.02$ μM) to inhibit BChE might be due to the presence of hydroxyl group in ring A. The inhibitory potential enhanced with the increase of olifinic double bond as in the case of compound **2** ($K_i = 2.5 \pm 0.04$ μM). The potency of compound **3** ($K_i = 18.0 \pm 0.04$ μM) decreased rapidly with the decrease of hydroxyl groups. Again potency increased sharply with the increase in the number of hydroxyl groups (compound **4**, $K_i = 2.2 \pm 0.02$ μM) as compared to compound **3** with the decrease of hydroxyl groups. There is a decrease in the potency of compound **5** ($K_i = 5.0 \pm 0.01$ μM) where there is no hydroxyl group on the ring A or B. The potency gradually increased when there is an increase of hydroxyl groups in compound **6** ($K_i = 4.6 \pm 0.06$ μM). Decrease in the number of hydroxyl moieties and olefinic bonds reduced the potency in the case of compound **7** ($K_i = 3.7 \pm 0.05$ μM) and compound **9** ($K_i = 4.2 \pm$

Table 3. Kinetic parameters of inhibition of AChE and BChE in the presence of compounds **1**–**9**

Compounds	AChE			BChE		
	$IC_{50} \pm$ SEM[a] [μM]	K_i[b] ± SEM [μM]	Type of inhibition	$IC_{50} \pm$ SEM [μM]	$K_i \pm$ SEM [μM]	Type of inhibition
1	8.3 ± 0.02	7.6 ± 0.01	NC	4.7 ± 0.01	4.5 ± 0.02	NC
2	0.89 ± 0.002	0.85 ± 0.001	NC	2.3 ± 0.01	2.5 ± 0.04	NC
3	1.0 ± 0.08	1.1 ± 0.05	NC	17.8 ± 0.05	18.0 ± 0.04	NC
4	17.2 ± 0.01	17.0 ± 0.02	NC	2.5 ± 0.02	2.2 ± 0.02	NC
5	26.4 ± 0.03	25.5 ± 0.01	NC	6.9 ± 0.02	5.0 ± 0.01	NC
6	19.2 ± 0.04	20.6 ± 0.02	NC	4.5 ± 0.02	4.6 ± 0.03	NC
7	15.2 ± 0.05	16.1 ± 0.01	NC	3.9 ± 0.06	3.7 ± 0.05	NC
8	13.7 ± 0.02	12.6 ± 0.04	NC	2.0 ± 0.05	2.5 ± 0.02	NC
9	3.5 ± 0.03	4.0 ± 0.09	NC	3.5 ± 0.01	4.2 ± 0.06	NC
Galanthamine[c]	0.5 ± 0.001	0.44 ± 0.0	MT	8.5 ± 0.00	8.0 ± 0.01	NC

NC, non-competitive; MT, mixed type.

[a] Standard means error of 3 assays.

[b] Dissociation constant or inhibition constant (determined from non-linear regression analysis by Dixon plot and secondary Lineweaver–Burk plot at various concentrations of compounds **1**–**9**).

[c] Standard inhibitor of AChE and BChE.

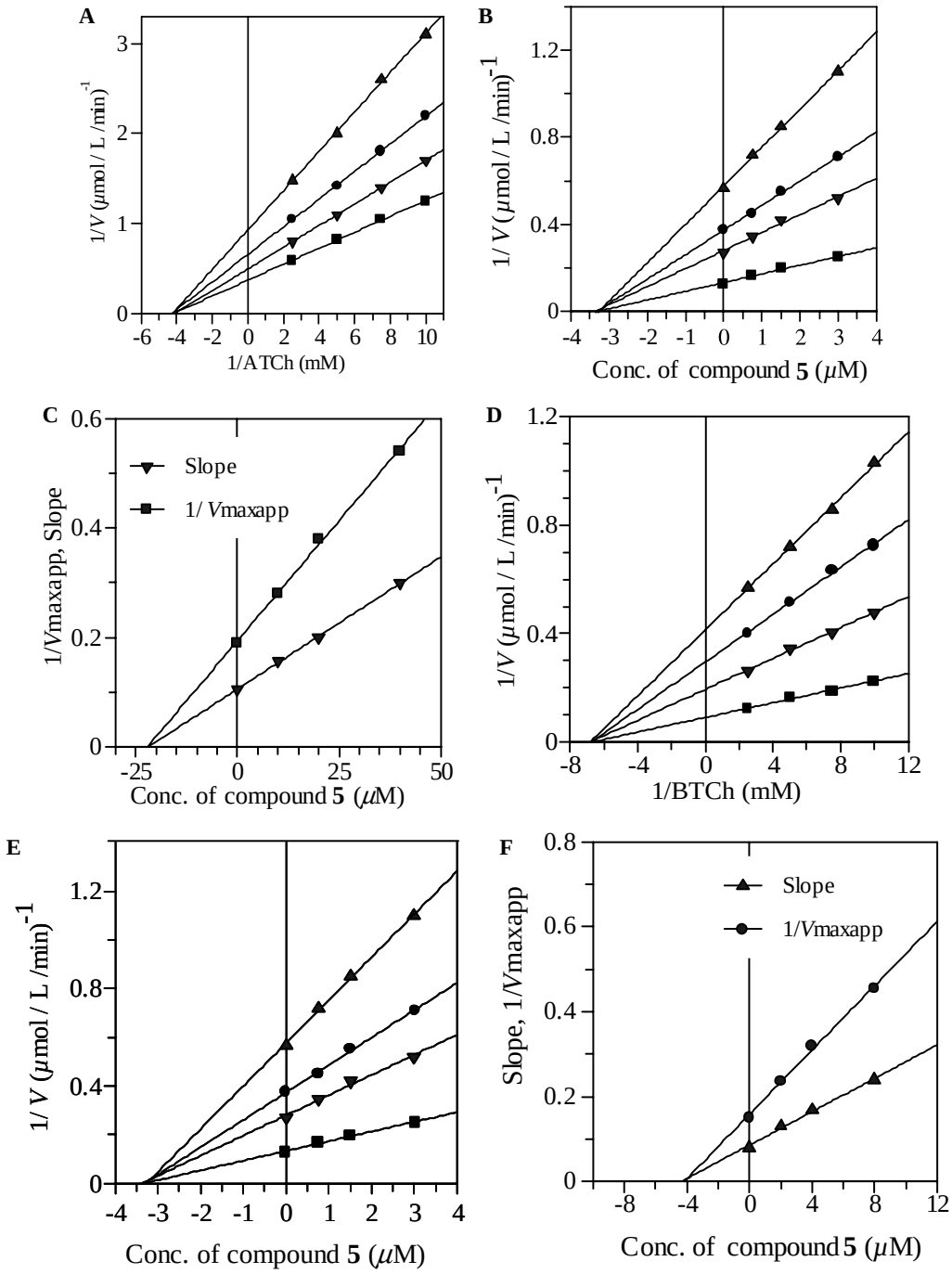

Figure 3. Steady-state inhibition AChE and BChE by compound **5**. (A) The Lineweaver–Burk plot of reciprocal of initial velocities versus reciprocal of four fixed ATCh concentrations in the absence (■) and presence of 10.0 μM (▼), 20.0 μM (●), and 40 μM (▲) of compound **5**. (B) The Dixon plot of reciprocal of the initial velocities versus various concentrations of compound **5** at fixed ATCh concentrations, (■) 0.4 mM, (▼) 0.2 mM, (●) 0.133 mM, and (▲) 0.1 mM. (C) The secondary replot of the Lineweaver–Burk plot, $1/V_{maxapp}$ or Slope versus various concentrations of compound **5**. (D) The Lineweaver–Burk plot of reciprocal of initial velocities versus reciprocal of four fixed BTCh concentrations in the absence (■) and presence of 2.5 μM (▼), 5.0 μM (●), and 7.5 μM (▲) of compound **5**. (E) The Dixon plot of reciprocal of the initial velocities versus various concentrations of compound **5** at fixed BTCh concentrations, (■) 0.2 mM, (▼) 0.1 mM, (●) 0.066 mM, and (▲) 0.05 mM. (F) The secondary replot of the Lineweaver–Burk plot, $1/V_{maxapp}$ or Slope versus various concentrations of compound **5**.

0.06 μM). A slight increase in the potency occurred with the increase of hydroxyl groups and olefinic bonds in compound **8** (K_i = 2.5 ± 0.02 μM).

The above discussion revealed that the activity pattern of compounds **1**–**9** against AChE and BChE depends both on the –OH and olefinic bonds. These functionalities seem to play a key role in the inhibitory potential of these compounds probably by making hydrogen bonds and π–π stacking interactions with the amino acid residues of the active center of the enzymes.

References and notes

1. Ali, S. I.; Qaiser, M. Flora of Pakistan, Department of Botany, University of Karachi, Karachi, Pakistan. **2001**; Vol. 204, p 185.
2. Sastri, B. N. The Wealth of India, Council of Scientific and Industrial Research, New Delhi **1959**; Vol. 5, p 5.
3. Jafri, S. M. H. Flora of Karachi, The Book Corporation, Karachi **1966**, p 99.
4. Nasir, E.; Ali, S. I. Flora of West Pakistan, Department of Botany, University of Karachi. **1978**; Vol. 121, p 2.
5. Stewart, R. R. An annotated catalogue of the vascular plants of West Pakistan and Kashmir, Flora of West Pakistan, Fakhri Press, Karachi, **1972**, p 223.
6. *Plant material*. The whole plant *Haloxylon recurvum* Bunge ex Boiss was collected from Cholistan desert near district Bahawalpur (Punjab), Pakistan, in October, 2001, and identified by Dr. Muhammad Arshad, Plant Taxonomist, Cholistan Institute of Desert Studies, Islamia University Bahawalpur, where a voucher specimen (020/CIDS/IUB/PK) has been deposited.
7. *Extraction and isolation*. The shade dried whole plant (20 kg) was exhaustively extracted with methanol (50 L × 3) at room temperature. The extract was evaporated to yield the residue (650 g), which was partitioned between *n*-hexane (60 g), chloroform (75 g), ethyl acetate (40.5 g), *n*-butanol (55 g), and water (25 g). The chloroform soluble fraction was subjected to column chromatography eluting with *n*-hexane-$CHCl_3$, $CHCl_3$, $CHCl_3$–MeOH in increasing order of polarity to afford fractions 1–12. Fraction 6 (7.5 g) was purified by column chromatography using *n*-hexane/$CHCl_3$ (3.0:7.0) as eluent to obtain lawsaritol (**7**) (25 mg) and (24*S*)-ethyl-cholesta-7,9(11),22(*E*)-triene-3β-ol (**6**) (18 mg), respectively. Fraction 8 was rechromatographed over silica gel eluting with *n*-hexane-$CHCl_3$ in increasing order of polarity. The fractions obtained from *n*-hexane/$CHCl_3$ (2.5:7.5) were subjected to preparative TLC (*n*-hexane/$CHCl_3$; 2.0:8.0) to afford haloxysterol B (**2**) (26 mg), 24-ethyl-cholest-6-ene-3,5-diol, (**9**) (19 mg) and 5α,8α-epidioxy-(24*S*)-ethyl-cholesta-6,9(11),22(*E*)-triene-3β-ol (**5**) (16.5 mg), respectively. Fraction 9 (15 g) was rechromatographed over silica gel eluting with *n*-hexane/$CHCl_3$ in increasing order of polarity to obtain fractions 9a, 9b, and 9c. The fraction 9b was further subjected to column chromatography eluting with *n*-hexane/$CHCl_3$ (1.0:9.0) to obtain haloxysterol C (**3**) (15 mg) from the top fractions and haloxysterol A (**1**) (14.5 mg) from the tail fractions. Fraction 11 was a mixture of two components which were separated by column chromatography using solvent system $CHCl_3$/MeOH (7.0:3.0), collecting 10 ml fractions in each case, to obtain haloxysterol D (**4**) (17 mg) from fractions 20 to 30 and 24-ethylcholest-7-ene-3,5,6-triol, (**8**) (19 mg) from fractions 60 to 70.
8. Haloxysterol A (**1**): White colorless crystals; mp 171–172 °C; $[\alpha]_D^{20}$ −63.5 (*c* 1, $CHCl_3$); IR (KBr) ν_{max} 3380, 1060, 885, 770 cm^{-1}. EIMS *m/z* (%): 446 $[M]^+$ (5), 428 $[M-H_2O]^+$ (14), 403 $[M-C_3H_7]$ (16), 389 $[M-C_3H_4O]^+$ (12), 377 (18), 363 (21), 319 (35), 317 (19), 289 (31), 157 (38), 83 (11), 127 (40), 57 (100), 43 (22). HREIMS *m/z* 446.3785 (calcd for $C_{29}H_{50}O_3$, 446.3760). ^1H NMR (400 MHz, $CDCl_3$) and ^{13}C NMR (100 MHz, $CDCl_3$) see Tables 1 and 2.
9. Haloxysterol B (**2**): White colorless crystals; mp 158–159 °C: $[\alpha]_D^{20}$ −55 (*c* 0.75, $CHCl_3$); UV λ_{max} (MeOH) ($\log\varepsilon$) nm: 232 (3.8), 240 (3.1), 248 (4.1). IR (KBr) ν_{max} 3440, 3390, 2960, 2855, 1676, 1380, 1265, 1120, 1080, 890 cm^{-1}. EIMS *m/z* (%): 444 $[M]^+$ (11), 426 $[M-H_2O]^+$ (28), 401 $[M-C_3H_7]^+$ (24), 389 $[M-C_3H_4O]^+$ (32), 363 (16), 317 (18), 292 (35), 287 (26), 129 (12), 81 (18), 55 (100), 43 (16), HREIMS *m/z* 444.3638 (calcd for $C_{29}H_{48}O_3$, 444.3603). ^1H NMR (400 MHz, $CDCl_3$) and ^{13}C NMR (100 MHz, $CDCl_3$) see Tables 1 and 2.
10. Haloxysterol C (**3**): White needles, mp 195 °C; $[\alpha]_D^{25}$ −75 (*c* 0.26, MeOH); UV λ_{max} (MeOH) ($\log\varepsilon$) nm: 238 (4.28) IR bands ν_{max} (KBr): 3390, 1686, 1610, 875 cm^{-1}. EIMS *m/z* (%): 426 $[M]^+$ 408 $[M-H_2O]^+$, 383 $[M-C_3H_7]^+$, 269 $[M-\text{side chain}]^+$ (100) 267 $[M-\text{side chain}-2H]^+$, 174 (42), 188 (38), 147 (28), 124 (35), 43 (98). HREIMS *m/z* 426.3471 (calcd for $C_{29}H_{46}O_2$, 426.3497). ^1H NMR (400 MHz, $CDCl_3$) and ^{13}C NMR (100 MHz, $CDCl_3$) see Tables 1 and 2.
11. Haloxysterol D (**4**): White crystals; mp 250–251 °C; $[\alpha]_D^{25}$ +35.5 (*c* 0.73, MeOH); IR (KBr) ν_{max}, 3444, 3392, 1070, 1050, 888, 776 cm^{-1}, Positive FABMS *m/z* 481 $[M+H]^+$, Negative FABMS *m/z* 479 $[M-H]^-$, EIMS *m/z* (%): 480$^+$ $[M]^+$, 464 $[M-H_2O]^+$, 449 $[M-H_2O-CH_3]^+$, 431 $[M-2H_2O-CH_3]$, 413 $[M-3H_2O-CH_3]^+$, 323 $[M-\text{side chain}]^+$, 322 $[M-\text{side chain}-H]^+$, 305 (100), 282 (28), 264 (33), 246 (23), 228 (28), 227 (18), 157 (22), 43 (58), HREIMS *m/z* 462.3735 (calcd for $C_{29}H_{50}O_4$, 462, 3709). ^1H NMR (400 MHz, Py-d_5) and ^{13}C NMR (100 MHz, Py-d_5) see Tables 1 and 2.
12. Findlay, J. A.; Patil, A. D. *Steroids* **1984**, *44*, 261.
13. Neal, A. C.; Prahl, F. G.; Eglinton, G.; O'Hara, S. C. M.; Corner, E. D. S. *J. Mar. Biol. Assoc. UK* **1986**, *66*, 1.
14. Gupta, S.; Ali, M.; Alam, M. S.; Niwa, M.; Sakai, T. *Phytochemistry* **1992**, *31*, 2558.
15. Piccialli, V.; Sica, D. *J. Nat. Prod.* **1987**, *50*, 915.
16. Greca, M. D.; Fiorentino, A.; Molinaro, A.; Monaco, P.; Previtera, L. *Nat. Prod. Lett.* **1994**, *5*, 7.
17. Quinn, D. M. *Chem. Rev.* **1987**, *87*, 955.
18. Perry, E. K. *Br. Med. Bull.* **1986**, *42*, 63.
19. Yu, S. Q. H.; Utsuki, H. W.; Brossi, T.; Greig, A. N. H. *J. Med. Chem.* **1999**, *42*, 1855.
20. Atta-ur-Rahman; Zaheer-ul-Haq, F. F.; Khalid, A.; Nawaz, S. A.; Choudhary, M. I. *Helv. Chem. Acta* **2004**, *87*, 439.
21. Khalid, A.; Choudhary, M. I.; Zaheer, H.; Anjum, S.; Khan, M. R.; Rahman, A. *Bioorg. Med. Chem.* **2004**, *12*, 1995.
22. Wyllie, S. G.; Amos, B. A.; Tokes, L. *J. Org. Chem.* **1977**, *42*, 725.
23. Holland, H. L.; Diakow, P. R. P.; Taylor, G. J. *Can. J. Chem.* **1978**, *56*, 3121.
24. Li, Y.; Ishibashi, M.; Satake, M.; Chen, X.; Oshima, Y.; Ohizumi, Y. *J. Nat. Prod.* **2003**, *66*, 698.
25. Letourneux, Y.; Khuong, H. Q.; Lukacs, G. *J. Org. Chem.* **1975**, *40*, 1674.
26. Scott, A. I. *Interpretation of the Ultraviolet spectra of Natural Products*; Pergamon Press: Oxford, 1964, 362.
27. Ahmad, S.; Nizami, T. A.; Nawaz, H. R.; Malik, A. Fitoterapia, **1998**, *LXIX*, 448.
28. Richa, P.; Verma, R. K.; Singh, S. C.; Gupta, M. M. *Phytochemistry* **2003**, *63*, 415.
29. Akihisa, T.; Kimura, Y.; Kokke, W. C. M. C.; Itoha, T.; Tamura, T. *Chem. Pharm. Bull.* **1996**, *46*, 1202.
30. Shoolery, J. N.; Rogers, M. T. *J. Am. Chem. Soc.* **1958**, *80*, 5121.
31. Yamada, Y.; Suzuki, S.; Iguchi, K.; Kikuchi, H.; Tsukitani, Y.; Horiai, H.; Nakanishi, H. *Chem. Pharm. Bull.* **1980**, *28*, 473.
32. *Cholinesterase inhibition assay*: The AChE and BChE inhibiting activities were measured by the spectrophotometric method developed by Ellman et al. 1962. Electric-eel AChE (EC 3.1.1.7), horse-serum BChE (E.C 3.1.1.8), acetylthiocholine iodide, butyrylthiocholine chloride, 5, 5′-dithiobis [2-nitrobenzoic acid] (DTNB), and galanthamine

were purchased from Sigma (St. Louis, MO, USA). All other chemicals were of analytical grade. Standard operational assay protocol has been described previously. All the kinetic experiments were performed in 96-well microtiter plates by using *SpectraMax 340* (Molecular Devices, CA, USA). The rate of the enzymatic reaction was measured by the following equation.

$$\text{Rate(mol/L/min)} = \frac{\text{Change in absorbance/min}}{13,600}$$

33. *Determination of kinetic parameters*. The concentration of compounds that inhibited the hydrolysis of substrates (acetylthiocholine and butyrylthiocholine) by 50% (IC_{50}) was determined by monitoring the effect of various concentrations of the compound in the assays on the inhibition values. The IC_{50} (inhibitor concn that inhibits 50% activity of AChE and BChE) values were then calculated using the EZ-Fit Enzyme Kinetics program (*Perrella Scientific Inc., Amherst*, USA). Dissociation constant/inhibition constant (K_i) was determined by the interpretation of Dixon plot, Lineweaver–Burk plot and their secondary replots using initial velocities obtained over a substrate concentration range between 0.1 and 0.4 mM for acetylthiocholine iodide (ATCh) and 0.05 and 0.2 mM for butyrylthiocholine chloride (BTCh). The dependency of V_{max}/K_m and V_{max} on inhibitor [I] is given by:

$$V_{max}/K_m = \left(\frac{(V_{max}/K_m)K_i}{K_i + [I]}\right)$$

Non-linear regression equations were used to determine the values of K_i, K_m, and V_{max} in the Lineweaver–Burk and Dixon plots. The K_i value [dissociation constant/inhibition constant of AChE–inhibitor or BChE–inhibitor complex into free AChE or BChE and inhibitor was determined graphically by Dixon and Lineweaver–Burk plots; first, $1/V_{maxapp}$ was calculated at each intersection point of lines of every inhibitor concentration on the *y*-axis of the Lineweaver–Burk plot and then replotted against various concentrations of inhibitors. Second, the slope of each line of inhibitor concentration on Lineweaver–Burk plot was plotted against inhibitor concentrations. Then replotting slope versus various concentrations of inhibitor, K_i is the intercept on *x*-axis.

34. *Statistical analysis*. Graphs were plotted using GraFit program. Values of the correlation coefficients, slopes, intercepts, and their standard errors were obtained by the linear regression analysis using the same program. The correlation of all the lines of all graphs was found to be >0.99. Each point in the constructed graphs represents the mean of three experiments.

35. Choudhary, M. I.; Devkota, K. P.; Nawaz, S. A.; Shaheen, F.; Atta-ur-Rahman *Helv. Chem. Acta* **2004**, *87*, 1099.
36. llman, G. L.; Courtney, K. D.; Andres, V.; Featherstone, R. M. *Biochem. Pharmacol.* **1961**, *7*, 88.
37. Dixon, M. *Biochem. J.* **1953**, *5*, 170.
38. Segel, H. I. *Non-competitive Inhibition (Simple intersecting linear non-competitive inhibition). In Enzyme Kinetics: Behavior and Analysis of Rapid Equilibrium and Steady State Enzyme Systems*; John Wiley: New York, 1993, pp. 101.
39. Leatherbarrow, R. J. GraFit Version 4.09, Erithacus Software Ltd. **1999**.